

# Thermal properties of poly(3-hydroxybutyrate) modified by nanoclay

Anna Czerniecka-Kubicka<sup>1</sup> · Wiesław Frącz<sup>2</sup> · Marek Jasiorski<sup>3</sup> · Wojciech Błażejowski<sup>3</sup> · Barbara Pilch-Pitera<sup>1</sup> · Marek Pyda<sup>1</sup> · Iwona Zarzyka<sup>1</sup>

Received: 15 March 2016 / Accepted: 5 December 2016 / Published online: 22 December 2016  
© The Author(s) 2016. This article is published with open access at Springerlink.com

**Abstract** Nanocomposites based on poly(3-hydroxybutyrate) (P3HB) and Cloisite<sup>®</sup>30B were prepared by direct mixing in a co-rotating twin-screw micro-extruder. The X-ray diffraction method and transmission electron microscopy allowed to identify the nanostructure. Thermal properties of the obtained nanocomposites were investigated with the use of thermogravimetry (TG) and differential scanning calorimetry (DSC). TG analysis of nanocomposites showed that thermal stability of the obtained nanocomposites was higher by approximately 20 °C than the neat P3HB. The phase transitions such as the glass transition, the crystallization and the melting have been studied by the DSC. The influence of nanofiller's presence in the polymer matrix on glass transition, crystallization and melting processes of the material obtained was determined and compared with the neat P3HB. The clay addition to the polymer matrix made the increase of the degree of crystallinity and the increase of the degree of amorphous of semi-crystalline P3HB. Furthermore, mechanical properties such as impact strength, flexural strength and hardness were investigated and compared with unfilled P3HB. Obtained nanocomposites containing

1 mass/% of Cloisite<sup>®</sup>30B have the best mechanical properties, better than the neat P3HB.

**Keywords** P3HB · Nanocomposites · Extrusion · Thermal properties · Mechanical properties

## Introduction

Recently, the biodegradable and biocompatible polymers are drawing a lot of attention because they are friendly to the environment. As a result, they have many biomedical applications, such as surgical materials, bridging and guiding materials for regenerating tissues such as nerve fibers and bones, scaffold material in repairing the atrial septal defect in calves, cardiovascular stents, barrier films for dental treatment, and micro-particulate carriers for drug delivery [1–10]. Biopolymers have been a very interesting field of research in comparison with conventional polymers, since they have been obtained from renewable resources. The degradation of conventional polymers is more difficult and the time of their application is very short, but they are still used to produce single-trip containers in agriculture.

Polyhydroxyalkanoates (PHAs) are naturally produced from various carbon substrates as carbon or energy reserve by microorganisms. PHAs are accumulated by a wide variety of prokaryotic organisms as cellular dry mass (from 30 to 80 mass%). One of the representatives of polyhydroxyalkanoates is poly(3-hydroxybutyrate) (P3HB) which is a fully biodegradable thermoplastic aliphatic polyester produced by many bacteria strains from cheap and renewable resources.

P3HB is a semi-crystalline polyester (above 50% of crystallinity) with a high melting point,  $T_m = 173\text{--}180$  °C,

✉ Iwona Zarzyka  
izarzyka@prz.edu.pl

<sup>1</sup> Faculty of Chemistry, Rzeszow University of Technology, Powstancow Warszawy 6, 35-959 Rzeszow, Poland

<sup>2</sup> Faculty of Mechanical Engineering and Aeronautics, Rzeszow University of Technology, Powstancow Warszawy 6, 35-959 Rzeszow, Poland

<sup>3</sup> Faculty of Mechanics, Wroclaw University of Science and Technology, M. Smoluchowskiego 25, 50-370 Wroclaw, Poland

in comparison with other biodegradable polyesters [11]. Its glass transition temperature ( $T_g$ ) is around 5 °C (0–27 °C) [12, 13]. The physical and mechanical properties of P3HB are compared with the isotactic polypropylene which made the P3HB a very attractive material [14]. Nevertheless, it has got several disadvantages: rigidity, brittleness and low thermal stability which nearly equals the melting temperature. These properties limit the commercial application of P3HB on a wide scale.

The thermal instability of this polymer in time of the melting process makes the replacement of the commercial non-biodegradable polymer with the P3HB difficult because of a narrow window for the processing conditions [15]. The establishment of thermal degradation process parameters provides particular information about internal structure of the polymer material [16, 17]. This problem is so crucial that the research in order to improve P3HB thermal stability should be conducted.

One of the methods to modify the properties of P3HB is the plasticization with citrate ester; these copolymers of P3HB are more adaptable for the process [12].

Among others, biosynthesis of copolymers with participation of other hydroxyalkanoate acid than 3-hydroxybutyrate acid, e.g., 3-hydroxyvalerate acid, was conducted [15, 18]. The next example is the preparation of the P3HB blend with other biodegradable polymers with suitable properties [11]. Moreover, block copolymers of P3HB are obtained in order to improve the properties of this latter [19].

Another possibility of the thermal stability enhancement is the preparation of nanocomposites containing P3HB. Nano-biocomposites are very interesting materials because they exhibit improved properties while maintaining a good degree of biodegradability of the material and non-toxicity [20]. These types of materials are mainly designed for biomedical applications and some short-term uses, for example to produce packs in agriculture or hygiene devices [18].

In many publications involving nanocomposites based on P3HB [21–30], the thermal decomposition kinetics have been studied using the TG method. Their thermal properties were not usually investigated by the DSC method. Erceg et al. [22, 23] studied the thermal degradation of nanocomposites containing P3HB and commercial montmorillonite modified by organic nanoclay—such as Cloisite 25A and Cloisite<sup>®</sup>30B produced by intercalation in solution. However, Achilias and co-workers have investigated the thermal decomposition of the nanocomposites containing P3HB and octadecylamine-modified montmorillonite prepared using an extruder [27]. Thermal studies of these nanocomposites have been performed using thermogravimetry analysis, and the kinetic analysis was performed using isoconversional method. In turn, Panayotidou

and co-workers studied biodegradation process and thermomechanical properties of nanocomposites of P3HB/montmorillonite. The last one was modified by octadecylammonium ions [21]. Nanocomposites were also obtained for P3HB matrix involving starch [28, 30], and lyocell or kenaf fiber [29], but these composites were tested only in respect of mechanical properties and biodegradation [29]. Vitorino et al. [20] investigated kinetics of non-isothermal melt crystallization of PHB composites based on babassu. Naguib et al. [31] tested properties of nanocomposites P3HB/Cloisite<sup>®</sup>30B by DSC, but composites were obtained by intercalation methods. Detailed thermal study of nanocomposites P3HB by DSC was conducted by Prakash et al. [32], wherein the nanofillers used were Cloisite C15A, C25A and C93A.

In this paper, new nanocomposites with the P3HB matrix and Cloisite<sup>®</sup>30B as nanofiller have been obtained with the use of co-rotating twin-screw micro-extruder. The structure of obtained nanocomposites was confirmed by the X-ray diffraction (XRD) and transmission electron microscopy (TEM) methods. The thermal properties of the obtained new nanocomposites were investigated by DSC method. Particularly, the effect of the nanofiller's presence (Cloisite<sup>®</sup>30B) on the glass transition temperature, melting temperature, change in the heat of fusion and the heat capacity change at  $T_g$ , and the impact of the nanofiller content on the change of these parameters were determined. Furthermore, the mechanical properties of the obtained nanocomposites were tested and compared with the neat P3HB.

## Experimental

### Materials

Poly(3-hydroxybutyrate) was supplied by Biomer (Krailling, Germany), and it was used as received. Its melt flow index was 0.11 g (10 min<sup>-1</sup>) (180 °C at 2.16 kg) and average molecular mass  $M_w = 1.600000$  g mol<sup>-1</sup> and dispersity  $M_w \cdot M_n^{-1} = 7.6$  as determined by size exclusion chromatography in chloroform. Organically modified montmorillonite Cloisite<sup>®</sup>30B was purchased from Southern Clay Products Inc. (Gonzales, USA). It is a natural montmorillonite modified with methylbis(2-hydroxyethyl)tallowalkylammonium cations.

### Preparation

The nanocomposites were prepared by melt mixing of P3HB with different amounts of Cloisite<sup>®</sup>30B (1, 2 and 3 mass/%) in a co-rotating twin-screw micro-extruder. The nanoclay was dried at 40 °C for 4 h under reduced pressure

and then dispersed in chloroform, water or ethylene glycol by ultrasonication at room temperature for 30 min. The dispersions were filtrated, and the clay was dried at 40 °C under reduced pressure. The melt mixing was carried out at conditions given in Table 1. Unfilled P3HB was also melt-mixed to prepare a reference material. Sample abbreviations and preparation conditions are given in Table 1.

## Structure and morphology characterization

### Scanning electron microscopy

Scanning electron microscopy was used for the characterization of the phase morphology of all prepared samples (i.e., P3HB, P3HB-1, P3HB-2 and P3HB-3 composites). The analyzed surfaces were previously coated with a thin layer of gold in a sputtering process. A HITACHI S-3400N scanning electron microscope equipped with an EDS system was used at various image magnifications and an accelerated voltage of 10 kV.

### SAXS analysis

Small-angle X-ray scattering (SAXS) measurements were taken at room temperature using X-ray diffractometer Bruker SAXS Nanostar-U. Comparative spectra for compression-molded samples were investigated in the transmission mode (coupled  $h\ 2\ h^{-1}$ ) to check the effect of the nanoparticles orientation. A small-angle goniometer was coupled to a sealed-tube source of filtered Cu K $\alpha$  radiation (1.54 Å) operating at 50 kV and 0.6 mA. The slit system enabled collection of diffracted beam with the divergence angle of less than 0.05. Measurements were taken in the range from 0 to 5 of the diffraction angle,  $2\theta$ .

### WAXS analysis

Wide-angle X-ray scattering (WAXS, 2D Phaser Bruker) was applied to gain information about the structural changes and phases of the obtained composites. A Cu K $\alpha$  ray was used for analysis. The scan rate was set to  $1^\circ\ \text{min}^{-1}$ ; the imposed voltage and current were 30 kV and

10 mA, respectively; and the diffraction angle ( $2\theta$ ) was varied from  $10^\circ$  to  $60^\circ$  at a rate of  $0.02^\circ\ \text{min}^{-1}$ .

### Transmission electron microscopy

Transmission electron microscopy (TEM) was used to study the nanostructure features of selected nanocomposites. TEM analysis of obtained composites was performed on a TECNAI G12 Spirit-Twin (LaB6 source) equipped with a FEI Eagle 4k CCD camera, operating with an acceleration voltage of 120 kV. Before the analysis, cryo-ultramicrotomed sections of the samples were realized and placed on 300-mesh copper grids.

### TG analysis

TG measurements were taken in Termowaga TGA/DSC 1 (Mettler) within 25–650 °C in open alumina crucibles. The measurement conditions were as follows: mass = 20–25 mg, heating rate  $q = 5^\circ\ \text{C}\ \text{min}^{-1}$ , with constant flow rate of around  $80\ \text{mL}\ \text{min}^{-1}$  nitrogen atmosphere.

### DSC measurements

Measurements were taken in the temperature range from  $-90$  to  $195^\circ\ \text{C}$  using two calorimeters: Q1000<sup>TM</sup> and TA 2920 from TA Instruments. These calorimeters are of heat flux type and use an external refrigerator to cool the sample. All experiments were performed in a nitrogen atmosphere with a constant flow rate of around  $50\ \text{mL}\ \text{min}^{-1}$ .

### Mechanical properties

Test specimens for mechanical properties were obtained by injection molding in accordance with DIN EN ISO 294-2 at a mold temperature of  $175^\circ\ \text{C}$ . The tested specimens were 4 mm in width and 10 mm in length. Charpy impact test was performed according to ISO 179 (Method A), while the flexural tests were performed at room temperature with a span distance equating 60 mm according to EN ISO 178: 1996. The flexural modulus was determined using a

**Table 1** Sample codes and preparation conditions of obtained nanocomposites

Sample designation	Content of Cloisite <sup>®</sup> 30B/mass/%	Solvent used for nanofiller dispersion	Temperature of extrusion/°C	Speed of rotation/rpm
P3HB-1	1	Water	170, 170, 170, 150	40
P3HB-2	2	Water		
P3HB-3	3	Water		
P3HB-3EG	3	Ethylene glycol		
P3HB-3C	3	Chloroform		

deformation rate of  $2 \text{ mm min}^{-1}$  and flexural strength with  $10 \text{ mm min}^{-1}$ .

Hardness test was realized using a Zwick Roell 3106 hardness tester according to DIN EN ISO 2039-1, with the ball diameter of 5 mm and 350 N of load. At least five specimens were used for each data point.

## Results and discussion

### Composite morphology: SEM and EDX observations

The morphology of P3HB and its composites containing 1, 2 and 3 mass/% of Cloisite<sup>®</sup>30B was observed by scanning electron microscopy (SEM) and is illustrated in Fig. 1a–d. The surface of neat P3HB is porous with an elongated structure (Fig. 1a). The surface porosity might be due to the presence of low molecular mass molecules, e.g., moisture, that are trapped inside the particles. The micrographs in Fig. 1b, c illustrate the very good and uniform dispersion of the nanoclay particles in the polymer matrix. The bright features in the figure represent the clay. The uniform distribution of nanoclay in the samples results from the relatively large gallery spacing of Cloisite<sup>®</sup>30B.

In order to investigate the distribution of Cloisite<sup>®</sup>30B particles in the P3HB nanocomposite matrix in more accurate way, energy-dispersive X-ray analysis (EDX, dot mapping of elements) was performed (Fig. 2). EDX analysis reflected the composition of the obtained hybrid organic–inorganic polymer composite, containing carbon, oxygen, silicon and aluminum. The mapping of the elements found on the SEM images (Fig. 2) by X-ray analysis allows to estimate the quantity of the elements in terms of atomic and mass percentages. The EDX analysis for all samples is summarized in Table 2.

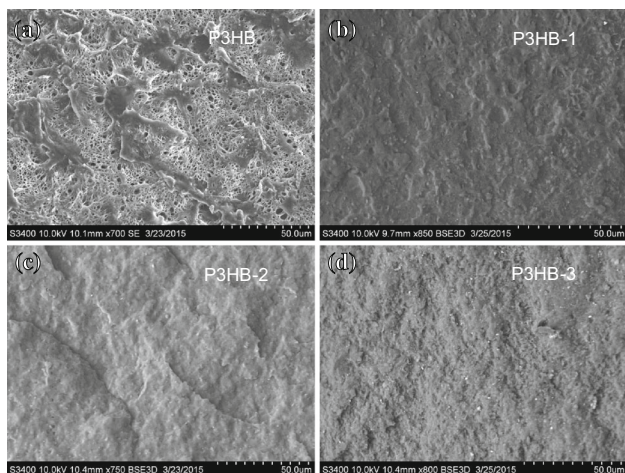


**Fig. 1** SEM photomicrograph of the samples: P3HB, P3HB-1, P3HB-2 and P3HB-3

Figure 2b–d shows the carbon, oxygen, silicon and aluminum atom distributions on the samples. The analysis shows a small increase in C atom percentages for composites P3HB-1 compared to neat P3HB and, next, the small decreasing of C content. This may be due to the presence of long chains of ammonium cations in the samples. The silicon atom percentage increases, as the Cloisite<sup>®</sup>30B is incorporated in larger amount and their distribution is still uniform. The aluminum atom presence is visible only in P3HB-3, i.e., in the case of highest content of Cloisite<sup>®</sup>30B. Probably, it results from the smaller amount of aluminum in the remaining composites.

### Nanostructure analyzed by X-ray diffraction

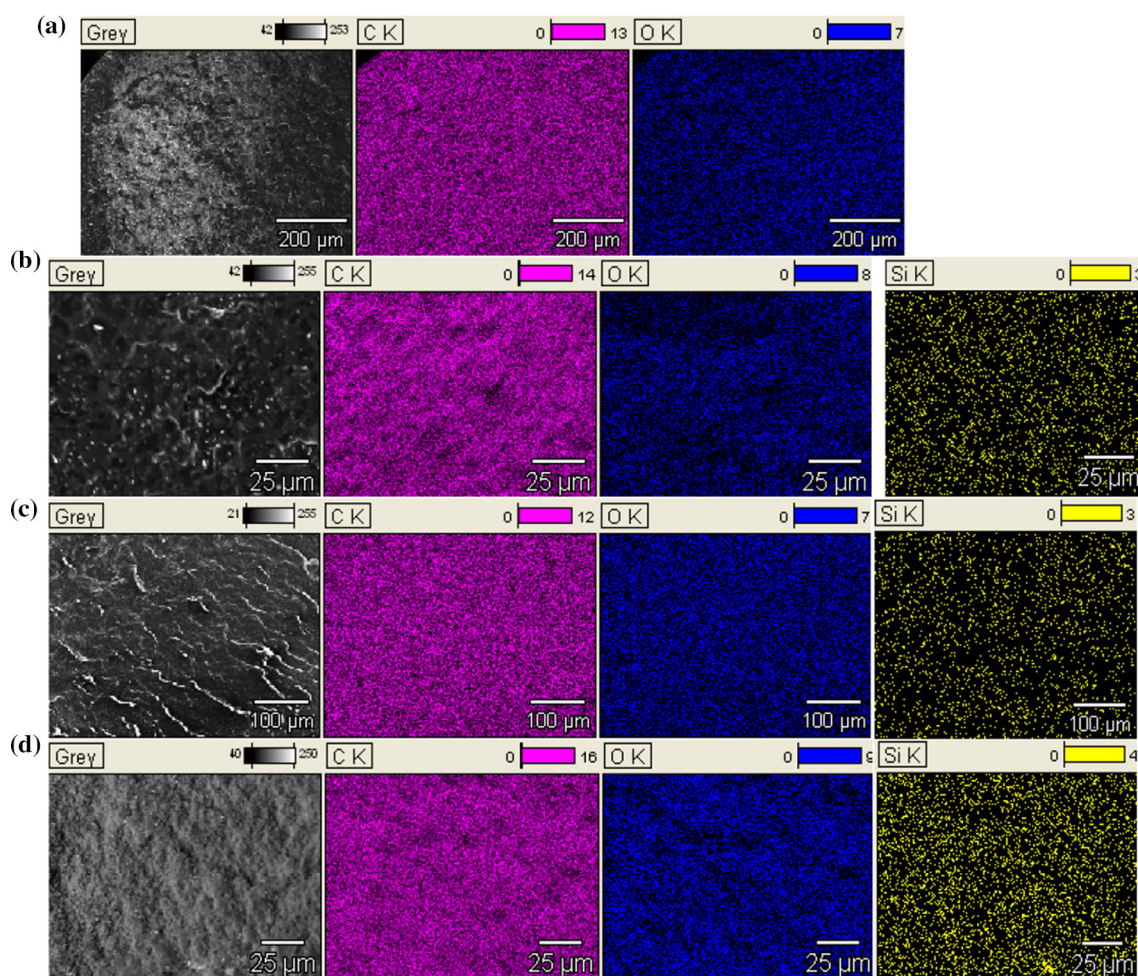
X-ray diffraction (XRD) technique was employed in the range  $1^{\circ}$ – $5^{\circ}$  to characterize the nanoclay structure within the prepared nanocomposites. The influence of the solvent type (water, chloroform, ethylene glycol), which was used for the nanofiller dispersion, on the structure of the resulting composites was investigated. It has been found that the best results are obtained by dispersing Cloisite<sup>®</sup>30B in water for 30 min.

Figure 3 shows diffractograms recorded for nanocomposites containing 3 mass/% of nanofiller dispersed in water, ethylene glycol and chloroform. For comparison, this figure contains also reference diffractograms of the unfilled P3HB and Cloisite<sup>®</sup>30B.

It is seen that the unfilled P3HB is characterized by background scattering with low intensity, while Cloisite<sup>®</sup>30B exhibits the diffraction maximum around  $2\theta = 4.92^{\circ}$  ( $d_{001} = 1.8 \text{ nm}$ ). All obtained nanocomposites show the diffraction maximum at a lower value  $2\theta$  than  $2^{\circ}$ . It means that P3HB chains penetrated between the layers of nanoclay stacks. It was observed that the increase of the interlayer distance depends on the solvent kind used for nanofiller dispersion. The lowest value  $2\theta$  has diffraction maximum of nanocomposites with nanofiller dispersed in water. Decreasing angle of diffraction is indicative of the intercalation of the layered silicate with the matrix constituents and the gallery spacing increasing. Bragg's equation ( $\lambda = 2d \cdot \sin\theta$ ) enables to calculate the interlayer spacing values ( $d_{001}$ ) between nanoclay plates. The diffraction maximum is situated at  $2\theta = 1.58, 1.25$  and  $1.1^{\circ}$ , i.e., the interlayer spacing values ( $d_{001}$ ) are 5.8, 6.4 and 6.8 nm for nanocomposites P3HB-3EG, P3HB-3C and P3HB-3, respectively.

Therefore, the further investigations were focused on nanocomposites with water-dispersed nanoparticles. No effect of the amount of water used for the dispersion of nanofillers on the structure of the resulting composites has been observed.





**Fig. 2** EDX dot mapping of **a** P3HB, **b** P3HB-1, **c** P3HB-2 and **d** P3HB-3 samples in respect of C, O and Si

**Table 2** EDX analysis results

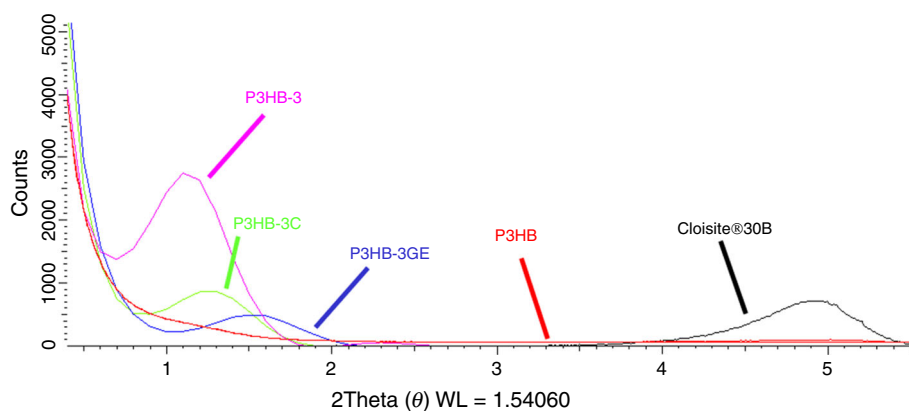
Mass%/at. %				
Element	P3HB	P3HB-1	P3HB-2	P3HB-3
C	59.73 (66.59)	60.35 (67.07)	59.07 (66.04)	58.20 (65.19)
O	39.56 (33.10)	39.41 (32.82)	40.43 (33.72)	40.84 (34.35)
Si	0	0.24 (0.11)	0.46 (0.24)	0.72 (0.34)
Al	0	0	0	0.24 (0.12)
Total	100	100	100	100

Figure 4 displays X-ray transmission spectra of nanocomposites P3HB-1, P3HB-2 and P3HB-3, respectively. The obtained nanocomposites show diffraction maximum at a lower value  $2\theta$  than diffraction maximum of Cloisite<sup>®</sup>30B, i.e., lower than  $1.2^\circ$ . This shift is as higher as lower organo-modified clay content in the polymer matrix is. The interlayer spacing values ( $d_{001}$ ) are 1.8 and 6.8 nm for the nanofiller and nanocomposite P3HB-3, respectively. It follows that the interlayer distance ( $\Delta d$ ) increased by 5 nm. The increase of the interlayer distance becomes

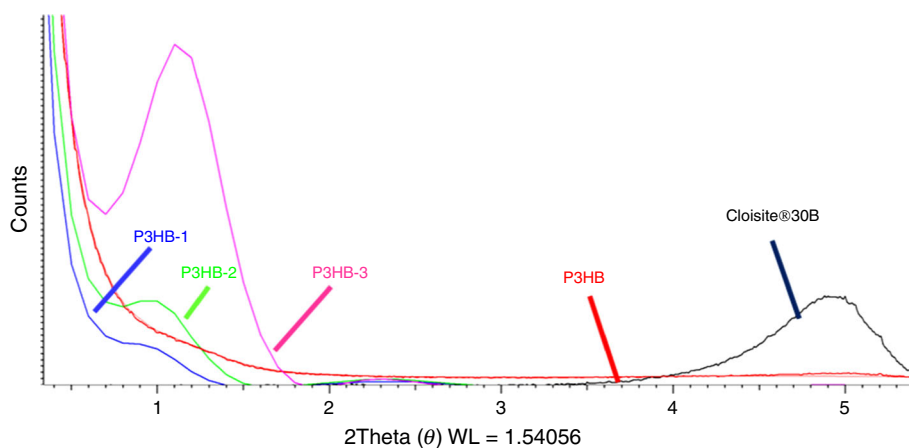
higher with the filler content decrease; the further shift of the maximum peak is observed. The presence of the peak at  $2\theta$  equal to approx.  $0.9^\circ$  and  $1^\circ$  on the diffractograms of composites containing 1 mass% (P3HB-1) and 2 mass% (P3HB-2) nanoclay indicates its good tactoids dispersion. It results from the intercalation and delamination of nanoplates in the P3HB matrix; the interlayer distance ( $d_{001}$ ) for P3HB-2 and P3HB-1 is 7.6 and 8.4 nm, respectively.

The diffractograms of obtained nanocomposites show that the small, second diffraction peak seen at  $2\theta = 2.33^\circ$

**Fig. 3** X-ray diffractograms recorded in the transmission mode for nanocomposites containing 3 mass% of clay dispersed in water, ethylene glycol and chloroform (they were marked as P3HB-3, P3HB-3EG, P3HB-3C, respectively). Reference spectra of unfilled P3HB and Cloisite®30B are also shown



**Fig. 4** X-ray diffractograms recorded in the transmission mode for nanocomposites containing 1, 2, and 3 mass% of clay dispersed in water (they were marked as P3HB-1, P3HB-2, P3HB-3, respectively). Reference spectra of unfilled P3HB and Cloisite®30B are also shown



corresponds with the second registry ( $d_{002}$ ). Its presence confirms the intercalated structure of the nanocomposites.

The analysis of the diffraction patterns proves a predominance of intercalated structure of nanocomposites, but a significant decrease in the intensity of the peaks confirming the intercalation (Fig. 4, P3HB-1 and P3HB-2) may indicate the formation of a disordered and/or exfoliated structure.

### Nanostructure analyzed by TEM

Nanocomposites were investigated by TEM to observe the effect of the preparation conditions, nanoclay content and processing conditions of nanoclay on the nanostructure features. The analysis of nanocomposites structure by TEM confirmed the conclusions resulting from XRD analysis of mentioned composites. The TEM micrographs show that Cloisite®30B is fairly susceptible to deagglomeration and dispersion in the P3HB matrix induced by shearing forces. Figure 5 shows examples of TEM images of nanocomposites obtained from nanofiller dispersed in chloroform, ethylene glycol and water (P3HB-3C, P3HB-3EG and P3HB-3), respectively. All nanocomposites images exhibit intercalated structure. Nevertheless, TEM images of the

nanocomposites containing water-dispersed Cloisite®30 (Fig. 5c) showed a higher degree of filler dispersion.

Therefore, the further investigations were focused only on these latter nanocomposites which contained different amounts of Cloisite®30B (P3HB-1, P3HB-2 and P3HB-3).

At larger magnification, the images (Fig. 6) show that the polymer penetrates the silicate gallery, increasing its intercalated distance (a few nanometers). The multilayered stacks are clearly discernible, but the whole delamination (exfoliation) on single silicate nanoplatelets is also possible in these systems. We should note that the individual silicate nanoplatelets and/or small stacks of only a few silicate nanoplatelets are not visible in the TEM. With decreasing nanofiller content, the size of dispersed regions of organoclay becomes smaller and smaller (Fig. 6).

### Thermal analysis of P3HB nanocomposites

In order to examine the durability of the obtained nanocomposites, i.e., in order to observe the physicochemical changes taking place upon heating, thermogravimetry (Fig. 7) and DSC analyses were performed (Figs. 8–10). TG analysis of nanocomposites showed that thermal stability of all nanocomposites is higher than that



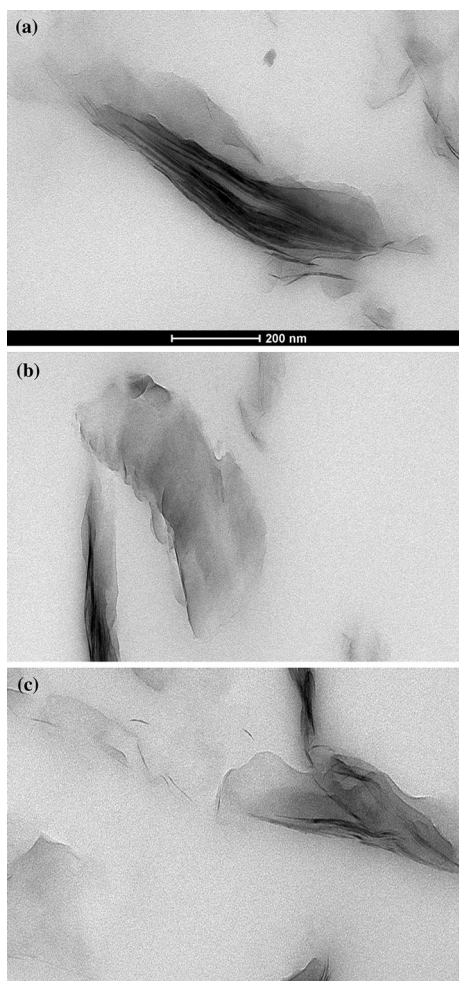


**Fig. 5** Example of TEM micrographs of nanocomposites containing 3 mass% of nanofiller which was dispersed in: **a** chloroform, **b** ethylene glycol, **c** water (P3HB-3C, P3HB-3EG, P3HB-3), respectively. Sections cut perpendicularly to the compression plane

of the neat P3HB. Introduction of Cloisite®30B into P3HB matrix causes the increase of the degradation temperature about 20 °C, e.g., 2% mass loss takes place at temperature 222.8 °C in the case of the neat P3HB and at 244.5, 244.0 and 243.3 °C in the case of P3HB-1, P3HB-2 and P3HB-3, respectively (Table 3). The mass loss temperature decreases with an increasing organo-modified clay content in the polymer matrix. At higher mass losses, the differences in the degradation temperature values are even higher. We can observe it, e.g., for the temperatures of the 10% mass loss—they equal 232.8, 256.7, 255.9 and 254.5 °C for P3HB and nanocomposites P3HB-1, P3HB-2 and P3HB-3, respectively.

In turn, Naguib examined composites P3HB/Cloisite®30B obtained by intercalation method and observed that the bigger additive of nanoclays caused the larger reduction in the decomposition temperature of the composite. It should be pointed out that he has applied 5

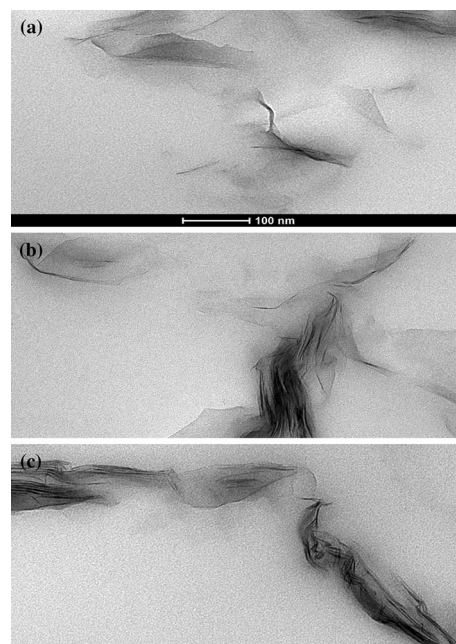


**Fig. 6** TEM micrographs of nanocomposites obtained from nanofiller dispersed in water containing 1, 2, 3 mass% of Cloisite®30B, respectively: **a** P3HB-1, **b** P3HB-2, **c** P3HB-3

and 10% Cloisite®30B and found only deterioration of the thermal properties of composites compared to neat P3HB (Table 3) [31].

### Study of the thermal properties of composites by DSC

The changes of the thermal properties of obtained composites were also studied using standard differential scanning calorimetry (DSC) (Figs. 9–14). The effect of the nanofiller additive on the glass transition temperature ( $T_g$ ), crystallization temperature and melting temperature ( $T_m$ ), and the variations of heat of fusion and the heat capacity at  $T_g$  were investigated. Figures 8 and 9 show the curves of the neat P3HB as well as its nanocomposites with a different content of nanofiller. Samples were cooled in a controlled way at a rate of 5 °C min<sup>-1</sup> from melt and after that were heated at rate of 10 °C min<sup>-1</sup>.

Based on a qualitative analysis (analysis of heat flow rate) of the neat semi-crystalline P3HB and its nanocomposites, the changes of heat capacity at  $T_g$  and heat of fusion at  $T_m$  and  $T_c$  were estimated. Parameters of phase transitions were estimated on the basis of changes of heat flow rate versus temperature in Figs. 8–10, and the values are shown in Table 4.

It can be observed that the values of glass transition, melting and crystallization temperature decreased with increasing contents of nanofillers. The change of glass transition and melting temperature reached 7 and 15 °C,

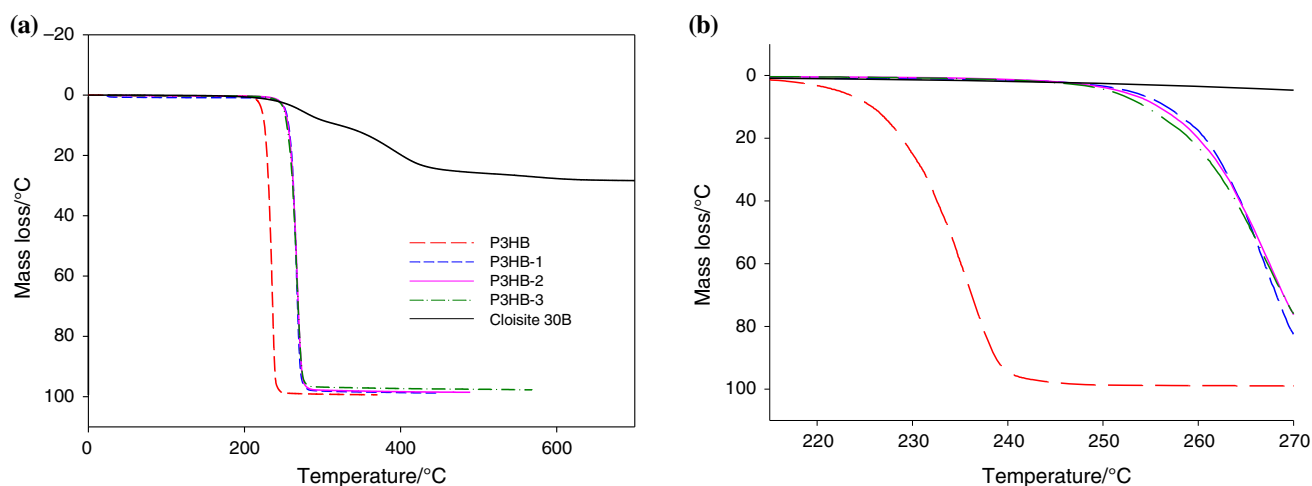


**Fig. 7** **a** TG analysis of the neat P3HB and their nanocomposites containing 1, 2 and 3 mass/% of clay (they were marked as P3HB-1, P3HB-2, P3HB-3, respectively). **b** An enlargement of the TG curves in the temperature range 220–280 °C

**Table 3** Thermal stability of P3HB and its nanocomposites (P3HB-1, P3HB-2, P3HB-3)

Name of sample	$T_{1\%}/^{\circ}\text{C}$	$T_{2\%}/^{\circ}\text{C}$	$T_{3\%}/^{\circ}\text{C}$	$T_{4\%}/^{\circ}\text{C}$	$T_{5\%}/^{\circ}\text{C}$	$T_{10\%}/^{\circ}\text{C}$
P3HB	215.4	222.8	226.0	227.8	229.2	232.8
P3HB-1	225.3	244.5	248.8	251.1	252.7	256.7
P3HB-2	236.9	244.0	248.3	250.5	251.8	255.9
P3HB-3	234.2	243.3	247.3	249.3	250.7	254.5

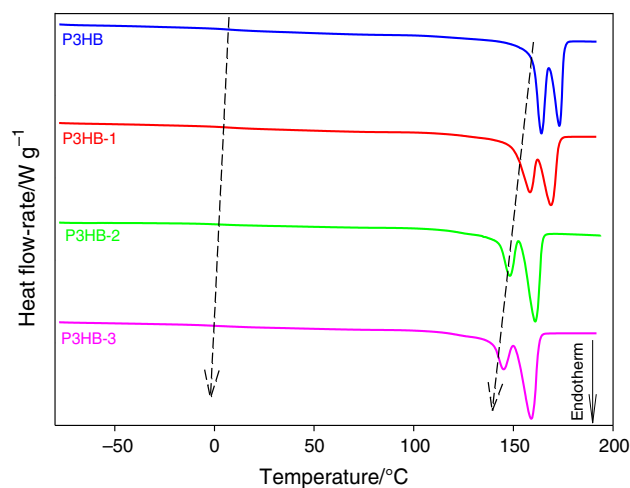


**Fig. 8** DSC analysis of the neat P3HB and its nanocomposites containing 1, 2 and 3 mass/% of clay (they were marked as P3HB-1, P3HB-2, P3HB-3, respectively). The results were obtained during heating at 10 °C/min after cooling the sample at a constant rate of 5 °C/min from melt

respectively. The variation of glass transition temperature for nanocomposite based on the highest amount of nanofiller in comparison with the neat P3HB equals 7 °C. These relationships confirm the good dispersion of nanofiller in the polymer matrix as reported earlier [24]. The decrease

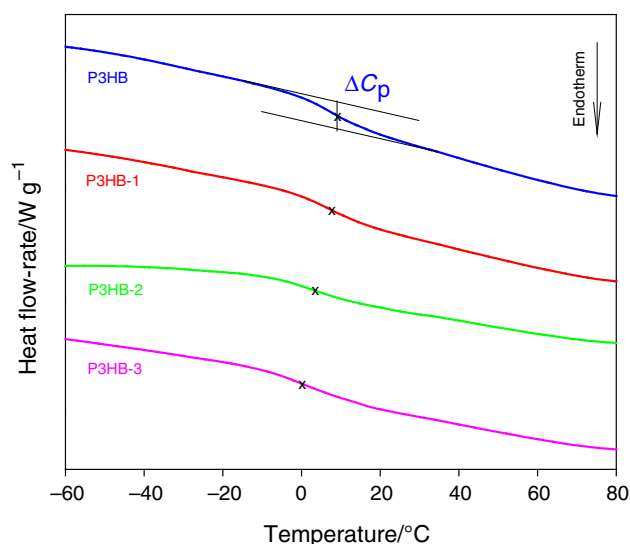


**Fig. 9** The inset shows the enlargement of the glass transitions in Fig. 2

of the glass transition temperature of the composite, compared to neat P3HB, with increasing amounts of introduced nanofiller indicates plasticizing effect of the filler. In turn, Naguib showed no change in glass transition temperature and only a slight decrease in the melting temperature with increasing amounts of Cloisite<sup>®</sup> 30B in



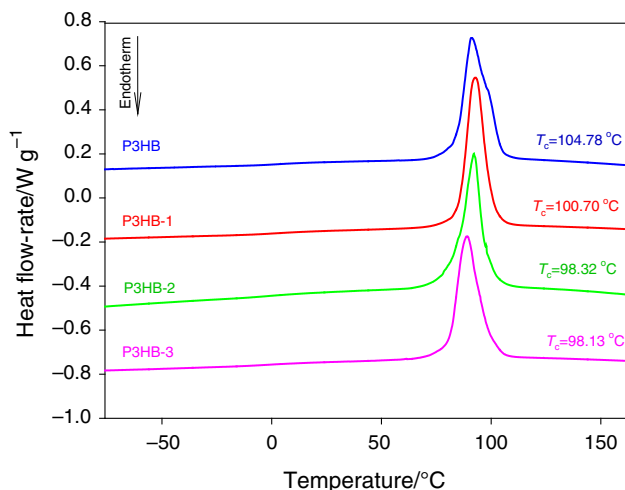


**Fig. 10** Crystallization analysis of the neat P3HB and its nanocomposites containing 1, 2 and 3 mass/% of clay (they were marked as P3HB-1, P3HB-2, P3HB-3, respectively). The results were obtained during cooling at a constant rate of 5 °C/min from melt

the polymer matrix. In contrast, the crystallization temperature while increasing the nanoadditive to 10 mass/% increased by 3 °C [31].

The substantial distinction between values of the degradation and melting temperature facilitates processing and prevents the degradation of the material. Moreover, we observe a little effect of nanofiller on the heat capacity, heat of fusion and heat of crystallization. Depending on different cooling rates, semi-crystalline P3HB's glass transition can be situated between 0 and 12 °C with a  $\Delta C_p$  (changes of heat capacity between liquid and solid states at  $T_g$ ) in the range 0.16–0.46 J °C<sup>-1</sup> g<sup>-1</sup>. The melting endotherm of semi-crystalline P3HB occurs between 155 and 172 °C with a heat of fusion in the range 3–97 J g<sup>-1</sup>.

Figure 11 shows the changes of heat capacity at the glass transition temperature and the measured heat of fusion for semi-crystalline P3HB samples with different thermal histories, after different cooling rate.

It should be noted that the changes of heat capacity values were estimated from qualitative thermal analysis (analysis of heat flow rate). The red points are characteristic of two-phase model. In turn, the blue points confirm the existence of the rigid amorphous fraction and characterized the three-phase model. The solid straight line is designated between full amorphous and full crystalline P3HB samples represented by circle green points. The change of heat capacity for fully amorphous P3HB equals 0.49 J g<sup>-1</sup> K<sup>-1</sup>, and the heat of fusion for fully crystalline samples equals 145 J g<sup>-1</sup>.

The dependence of the mobile amorphous fraction on the degree of crystallinity of semi-crystalline neat P3HB is shown in Fig. 12. The data obtained from Fig. 8 were converted to corresponding degree of amorphous phase (Eq. 1) and degree of crystallinity (Eq. 2). The pink point

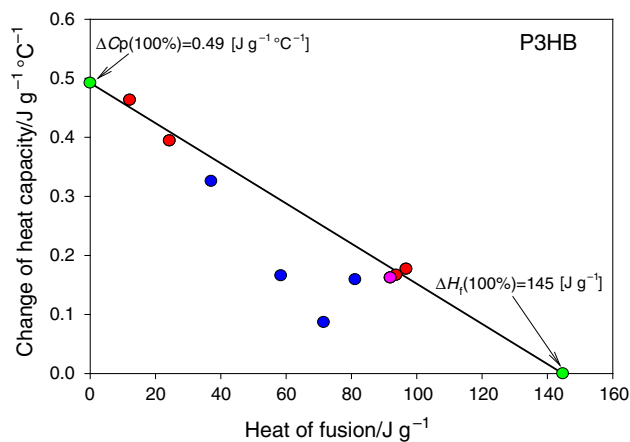


**Fig. 11** Plot of heat capacity changes at glass mobile transition temperature versus heat of fusion of semi-crystalline P3HB with different thermal histories (the various cooling rates were applied). The red points are characteristic of two-phase model; the blue points show the rigid amorphous fraction and characterize the three-phase model. The solid straight line is designated between full amorphous and full crystalline P3HB samples represented by circle green points

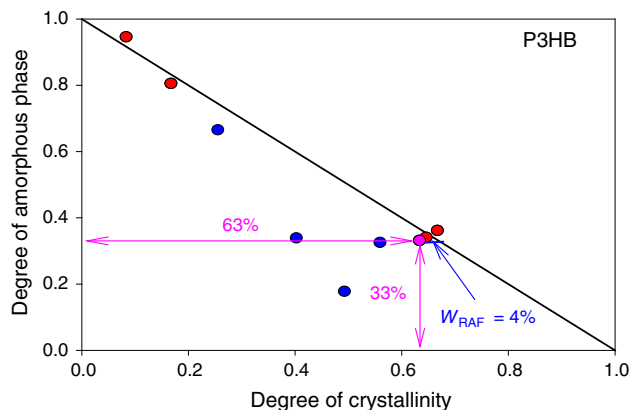


**Fig. 12** Dependence of the amorphous fraction as a function of the degree of crystallinity of the semi-crystalline neat P3HB (denoted by P3HB). The red points are characteristic of two-phase model of polymer, and the blue points show the three-phase model of P3HB. The pink point derived from qualitative analysis of the neat P3HB was obtained during heating at 10 °C/min after cooling the sample at a constant rate of 5 °C/min from the melt

derived from qualitative analysis of the neat P3HB is also plotted in Figs. 11 and 12. The data of this pink point were obtained during heating at 10 °C min<sup>-1</sup> after cooling the sample at constant rate 5 °C min<sup>-1</sup> from the melt.

The mobile amorphous fraction ( $W_a$ ) was estimated using thermal analysis from equation:

$$W_a = \frac{\Delta C_p}{\Delta C_p^{100\%}} \quad (1)$$

where  $\Delta C_p$  and  $\Delta C_p^{100\%}$  are variations of heat capacity at  $T_g$  (mobile) of semi-crystalline and full amorphous P3HB, respectively. For computation, the value of  $\Delta C_p^{100\%} = 0.49 \text{ J K}^{-1} \text{ g}^{-1}$  was used.

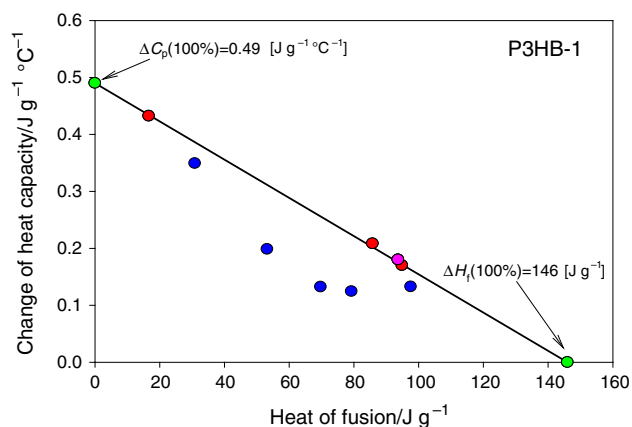


**Fig. 13** Dependence of the heat capacity change at the glass transition temperature versus the heat of fusion of the semi-crystalline nanocomposites P3HB containing 1 mass/% of clay (denoted as P3HB-1). The *red points* are characteristic of two-phase model of nanocomposite, and the *blue points* show the three-phase model of P3HB-1. The *solid straight line* is designated between full amorphous and full crystalline P3HB-1 samples represented by *circle green points*. The *pink point* derived from qualitative analysis of the neat P3HB-1 was obtained during heating at 10 °C/min after cooling the sample at a constant rate of 5 °C/min from the melt

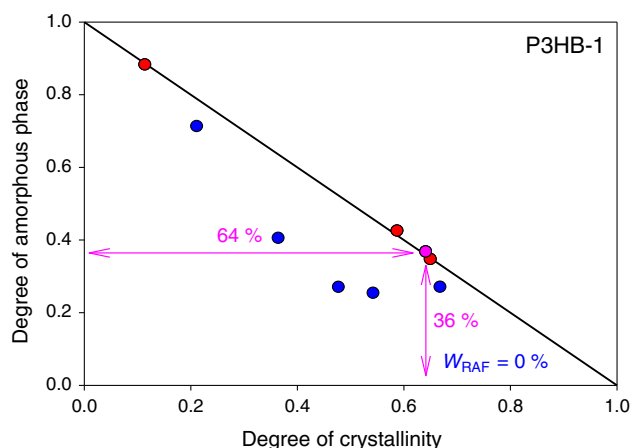


**Fig. 14** Dependence of the amorphous fraction as a function of the degree of crystallinity of the semi-crystalline P3HB nanocomposite containing 1 mass/% of clay (denoted as P3HB-1)

The degree of crystallinity ( $W_c$ ) was defined as the ratio between experimental heat of fusion ( $\Delta H_f$ ) of the semi-crystalline sample and heat of fusion of the fully crystalline P3HB sample ( $\Delta H_f^{(100\%)}$ ) as follows:

$$W_a = \frac{\Delta H_f}{\Delta H_f^{100\%}} \quad (2)$$

It has been calculated that selected P3HB sample (pink points) remains in a three-phase model which is confirmed in Fig. 12 (the sample shows deviation from a straight line). As illustrated in Fig. 12, P3HB contains 33% amorphous, 63% crystalline phase and 4% rigid amorphous fraction.

Figure 13 shows the examples of the changes of heat capacity at the glass transition temperature and the measured heat of fusion for nanocomposites containing 1 mass/% of clay (denoted as P3HB-1) obtained after different cooling rates.

The values in this plot were derived from qualitative thermal analysis. The red points are characteristic of two-phase model. In turn, the blue points indicate the existence of the rigid amorphous fraction and confirm the presence of the three-phase model. The solid straight line is designated between full amorphous and full crystalline sample of nanocomposites represented by circle (green points).

Figure 14 shows dependence of the amorphous fraction as a function of the degree of crystallinity for the semi-crystalline P3HB nanocomposites containing 1 mass/% of clay. The dependence of the heat capacity change at the glass transition temperature versus the heat of fusion of the semi-crystalline P3HB and its other nanocomposites was estimated like for the neat P3HB and P3HB-1. The change of heat capacity for fully amorphous material and the heat of fusion for fully crystalline material were also obtained in the same method like for the neat P3HB. The phase contents of nanocomposites were calculated in similar way like the neat P3HB. Obtained results for all nanocomposites are listed in Table 5.

In Table 5, the phase contents are calculated for samples which in a controlled way at a rate of 5 °C min<sup>-1</sup> were cooled and after that were heated at a rate of 10 °C min. Based on those results, it can be concluded that the addition of nanoclay leads to the increase of the degree of crystallinity of nanocomposites. Naguib observed the opposite situation, i.e., the degree of crystallinity decreased with the increase of the content Cloisite<sup>®</sup>30B [31]. The differences between our study and literature observation [31] were

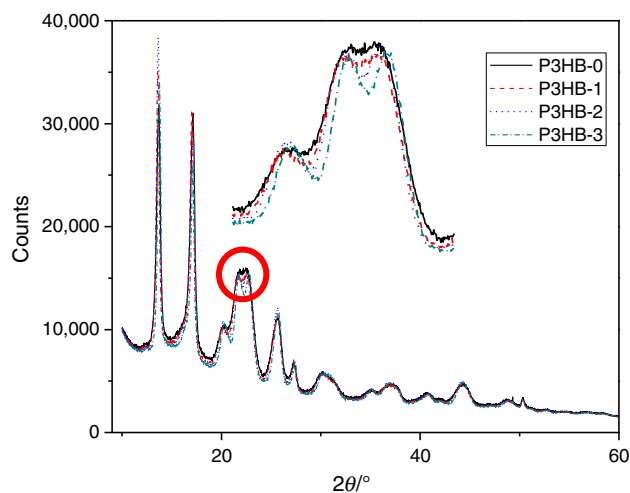
**Table 4** Characterization of thermal properties of P3HB and its nanocomposites (P3HB-1, P3HB-2, P3HB-3)

Name of sample	$T_g/^\circ\text{C}^a$	$\Delta H_f/\text{J g}^{-1}$	$T_m/^\circ\text{C}^a$	$\Delta C_p/\text{J g}^{-1} \text{ }^\circ\text{C}^{-1}$	$T_{m1}/^\circ\text{C}^a$	$T_{m2}/^\circ\text{C}^a$	$\Delta H_f/\text{J g}^{-1}$
P3HB	104.78	88.79	7.69	0.1621	159.69	172.20	91.93
P3HB-1	100.70	94.36	7.48	0.1714	157.73	160.55	93.69
P3HB-2	98.32	95.31	3.35	0.1650	147.34	161.06	95.70
P3HB-3	98.13	84.56	0.35	0.1600	144.41	158.93	98.60

<sup>a</sup> The values of temperature equal the onset temperature

**Table 5** Characterization of phase contents for the neat P3HB and its nanocomposites

Name of sample	$\Delta C_p$ (100%)/J g <sup>-1</sup> °C <sup>-1</sup>	$\Delta H_f$ (100%)/J g <sup>-1</sup>	$W_c$ /%	$W_d$ /%	$W_{RAF}$ /%
P3HB	0.49	145	63	33	4
P3HB-1	0.49	146	65	35	0
P3HB-2	0.50	145	66	33	1
P3HB-3	0.50	145	68	32	0

**Fig. 15** WAXS diffractograms of nanocomposites containing 1, 2 and 3 mass% of clay; they were marked as P3HB-1, P3HB-2, P3HB-3, respectively. Reference spectra of unfilled P3HB and Cloisite<sup>®</sup>30B are also shown. The *inset* shows the magnification of the diagnostic area from 19 to 24

probably caused by the various contents of nanofiller in the investigated polymer matrix. Naguib and co-workers used a very large amount of nanofiller (5–10%), and they probably have not received adequate mixing of ingredients. Furthermore, only small content of nanofiller (1–5%) improves properties of nanocomposite. Otherwise, the agglomeration of the nanofiller particles can occur. It changes properties of materials on disadvantage.

Additionally, it can be ascertained that addition of clay to the polymer matrix did not sufficiently change heat capacity  $\Delta C_p^{(100\%)}$  at the glass transition temperature for fully amorphous samples and the heat of fusion  $\Delta H_f^{(100\%)}$  of nanocomposites for fully crystalline samples.

Figure 15 shows WAXS spectra of neat P3HB and its nanocomposites. The spectra indicate a gradient of increased resolution and peak sharpness with increased amount of nanoclay in composites. In the enlargement of spectrum in the range from 19 to 24, the peak resolution increases. It indicates a crystallinity growth of obtained nanocomposites. This phenomenon is due to the increase in crystal number as the organoclay percentage increases.

## Mechanical properties

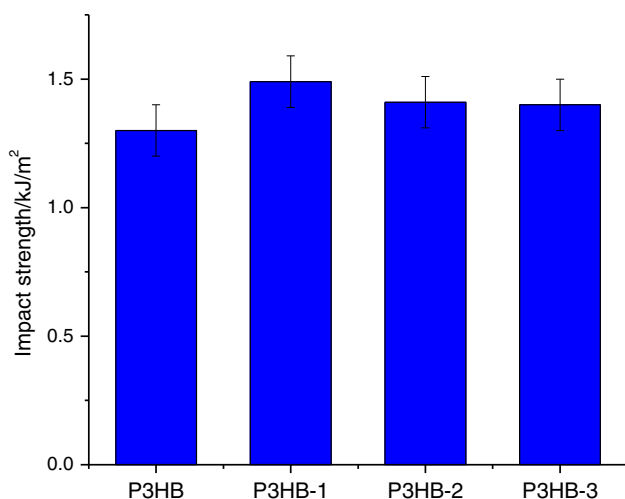
The following mechanical properties of the obtained nanocomposites were investigated: impact strength, flexural strength and hardness.

Average impact strength (IS) values of the obtained nanocomposites are presented in Fig. 16. It can be noted that all modified composites showed higher IS than virgin sample. However, maximum impact strength (15% improvement in comparison with neat P3HB composite) was exhibited by composite designated P3HB-1 (composite based on 1 mass% of Cloisite<sup>®</sup>30B). It should be pointed out that IS of P3HB-2 and P3HB-3 was higher than that of neat P3HB, but the IS increase was not significant. The improvement of the nanocomposites impact strength in the case of P3HB-1 is due to the highest exfoliation and/or intercalation of incorporated nanoclay.

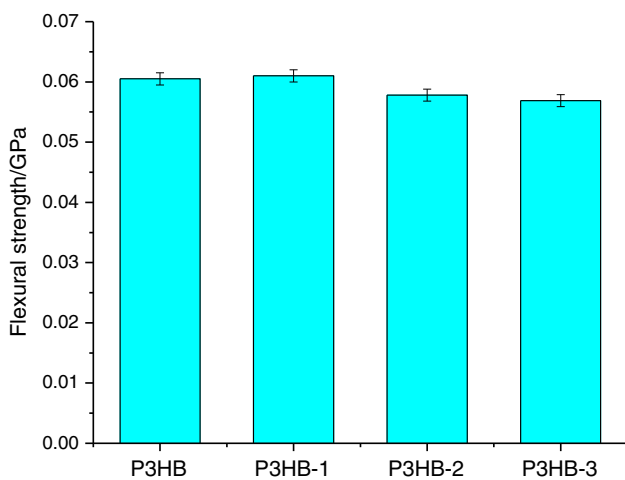
From Fig. 17, it can be shown that the flexural strength of P3HB-1 exhibited slightly higher value than unfilled P3HB and all other nanocomposites. However, it should be mentioned that the presence of nanofiller did not affect the flexural strength value. On the other hand, we can suppose that the greatest impact of nanofiller on flexural strength takes place while the composite containing less than 1 mass% of nanofiller.

Figure 18 represents the flexural modulus of all prepared composites. The modulus values of nanocomposite containing 1 mass% nanoclay (composite P3HB-1) increased by approximately 20% in relation to non-modified sample. Further increase of nanofiller content caused a decrease in flexural modulus values, but they were still higher than that of neat P3HB. Obtained P3HB nanocomposites exhibited intercalated structure, but the decreasing nanofiller content resulted in smaller and smaller size of dispersed organoclay and exfoliated or mixed structures. Therefore, the best mechanical properties were exhibited by the composite designated P3HB-1.

From Fig. 19, it can be observed that the introduction of Cloisite<sup>®</sup>30B in P3HB matrix caused usually an increase of hardness of the tested material. However, the hardness of the composite P3HB-1 was almost unchangeable compared to neat P3HB. The highest variation was observed for the



**Fig. 16** Impact strength of prepared composites



**Fig. 17** Flexural strength of obtained composites

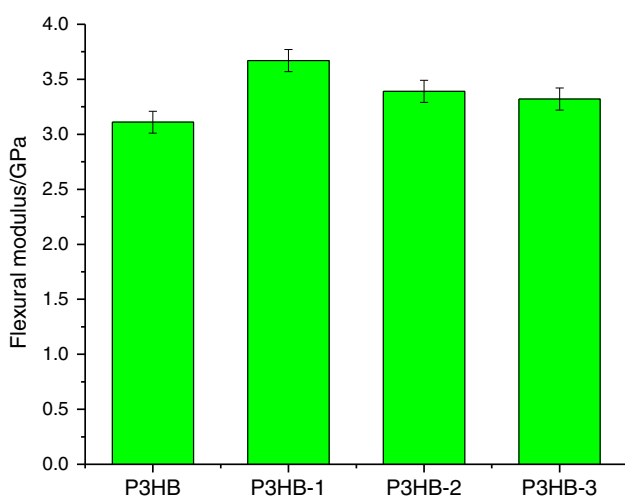


**Fig. 18** Flexural modulus of composites containing different amounts of nanoclay

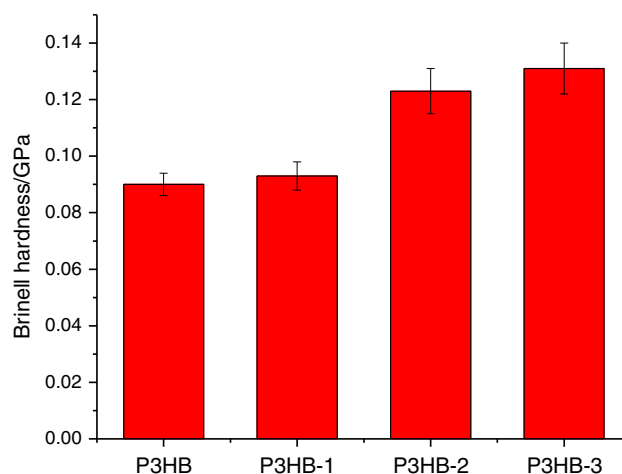


**Fig. 19** Average values of Brinell hardness test based on the content of Cloisite®30B

composite P3HB-2 and attained about 35% compared to neat P3HB.

## Conclusions

The nanocomposites of P3HB and Cloisite®30B were obtained. The P3HB matrix penetrated within the layered silicate galleries of Cloisite®30B and intercalation took place, but semi-exfoliation cannot be excluded. This was possible due to strong interaction between the components and shearing forces during direct mixing in a co-rotating twin-screw micro-extruder. The structure of obtained nanocomposites was confirmed by TEM analysis and XRD.

The conducted studies revealed clearly the influence of organoclay dispersion in the P3HB matrix on the selected thermal and mechanical properties of the prepared nanocomposites.

It has been observed that the introduction of the nanoplates into polymer matrix influences the better thermal stability of the nanocomposites, measured by TG, under non-oxidative conditions. With an increase of the nanoplates concentration, the thermal stability of the nanocomposites was better than that of the neat P3HB.

The presented thermal analysis showed a decrease in the glass transition, melting and crystallization temperatures with an increasing amount of nanofillers in the obtained P3HB composites. The decrease in the melting point of the composites is preferred due to the fact that the melting point of the neat P3HB is close to its decomposition temperature. This movement apart from melting and decomposition temperatures of composites based on P3HB facilitates processing and prevents the degradation of the material.



Additionally, introducing nanoclay into the P3HB material leads to the increase of the degree of crystallinity of nanocomposites. WAXS spectra confirmed a crystallinity growth of obtained nanocomposites. This phenomenon is due to the increase in crystal number as the organoclay percentage is higher.

Poly(3-hydroxybutyrate)-based nanocomposites prepared using an extrusion process showed improved impact strength, flexural modulus and slightly flexural strength. The best mechanical properties were exhibited by the composite designated 1 mass/% of nanofillers. The impact strength of nanocomposite P3HB containing 1 mass/% of Cloisite<sup>®</sup>30B increased by 15% in comparison with non-modified polymer. In turn, the flexural modulus value increased by approximately 20%. Obtained composites containing the smallest amount of nanofillers—only 1 mass/%—have the smallest size of dispersed organoclay. It resulted in the most participation of exfoliated structure of obtained composites and the best mechanical properties.

We can assume that the composite containing less than 1% by mass of Cloisite<sup>®</sup>30B could have even better properties, but it will be the focus of our future research.

**Acknowledgements** X-ray analysis was performed in the Laboratory of Spectrometry, Faculty of Chemistry, Rzeszow University of Technology, and was financed from DS budget. The authors would like to thank Maria Laura Di Lorenzo and Gennaro Gentile from Consiglio Nazionale delle Ricerche, Istituto di Chimica e Tecnologia dei Polimeri, c/o Compresorio Olivetti, Via Campi Flegrei 34, 80078 Pozzuoli (NA), Italy, for TEM analysis of nanocomposites.

**Open Access** This article is distributed under the terms of the Creative Commons Attribution 4.0 International License (<http://creativecommons.org/licenses/by/4.0/>), which permits unrestricted use, distribution, and reproduction in any medium, provided you give appropriate credit to the original author(s) and the source, provide a link to the Creative Commons license, and indicate if changes were made.

## References

- Chen GQ, Wu Q. The application of polyhydroxyalkanoates as tissue engineering materials. *Biomaterials*. 2005;26:6565–78.
- Chen GQ. A microbial polyhydroxyalkanoates (PHA) based bio-materials industry. *Chem Soc Rev*. 2009;38:2434–46.
- Brigham CJ, Sinskey AJ. Applications of polyhydroxyalkanoates in the medical industry. *Int J Biotech Wellness Ind*. 2012;1:53–60.
- Bowald SF, Johansson EG. A novel surgical material. *EP 0349505 A 2* (1990).
- Malm T, Bowald S, Bylock A, Busch C. Prevention of postoperative pericardial adhesions by closure of the pericardium with absorbable polymer patches: an experimental study. *J Thorac Cardiovasc Surg*. 1992;104:600–7.
- Duvernoy O, Malm T, Ramstrom J, Bowald S. A biodegradable patch used as a pericardial substitute after cardiac surgery: 6- and 24-month evaluation with CT. *Thorac Cardiovasc Surg*. 1995;43:271–4.
- Hazari A, Johansson-Rudén G, Junemo-Bostrom K, Ljungberg C, Terenghi G, Green C, Wiberg M. A new resorbable wrap-around implant as an alternative nerve repair technique. *J Hand Surg*. 1999;24:291–5.
- Kostopoulos L, Karring T. Guided bone regeneration in mandibular defects in rats using a bioresorbable polymer. *Clin Oral Implan Res*. 1994;5:66–74.
- Kostopoulos L. Augmentation of the rat mandible using guided tissue regeneration. *Karring Trans Clin Oral Implan Res*. 1994;5:75–82.
- Malm T, Bowald S, Karacagil S, Bylock A, Busch C. A new biodegradable patch for closure of atrial septal defect: an experimental study. *Scand J Thorac Cardiovasc Surg*. 1992;26:9–14.
- Janigová I, Lacík I, Chodák I. Thermal degradation of plasticized poly(3-hydroxybutyrate) investigated by DSC. *Polym Degrad Stab*. 2002;77:35–41.
- Schick C, Wurm A, Mohammed A. Vitrification and devitrification of the rigid amorphous fraction of semicrystalline polymers revealed from frequency-dependent heat capacity. *Colloid Polym Sci*. 2001;279:800–6.
- Wei Z, Liu L, Qi M. Synthesis and characterization of homo- and co-polymers of (R, S)- $\beta$ -butyrolactone and  $\gamma$ -butyrolactone or  $\beta$ -valerolactone initiated with cyclic tin alkoxide. *React Funct Polym*. 2006;66:1411–9.
- Fernandes EG, Pietrini M, Chiellini E. Thermo-mechanical and morphological characterization of plasticized poly [(R)-3-hydroxybutyric acid]. *Macromol Symp*. 2004;218:157–64.
- Lee SN, Lee MY, Park WH. Thermal stabilization of poly(3-hydroxybutyrate) by poly(glycidyl methacrylate). *J Appl Polym Sci*. 2002;83:2945–52.
- Pagacz J, Pielichowski K. Preparation and characterization of PVC/montmorillonite nanocomposites—a review. *J Vinyl Addit Technol*. 2009;15:61–76.
- Achillas DS, Karabela MM, Sideridou ID. Thermal degradation and isoconversional kinetic analysis of light-cured dimethacrylate copolymers. *J Therm Anal Calorim*. 2010;99:917–23.
- Lehrle R, Williams R, French C, Hammond T. Thermolysis and methanolysis of poly(beta-hydroxybutyrate)—random scission assessed by statistical-analysis of molecular-weight distributions. *Macromolecules*. 1995;28:4408–14.
- Li G, Liu Y, Li D, Zhang L, Xu K. A comparative study on structure-property elucidation of P3/4HB and PEG-based block polyurethanes. *J Biomed Mater Res A*. 2012;100:2319–29.
- Vitorino M, Cipriano P, Wellen R, Canedo E, Carvalho L. Nonisothermal melt crystallization of PHB/babassu compounds Kinetics of crystallization. *J Therm Anal Calorim*. 2016. doi:10.1007/s10973-016-5514-7.
- Panayotidou E, Baklavariadis A, Zuburtikudis I, Achillas DS. Nanocomposites of poly(3-hydroxybutyrate)/organomodified montmorillonite: effect of the nanofiller on the polymer's biodegradation. *J Appl Polym Sci*. 2015;132:41656–63.
- Erceg M, Kovacic T, Perinovic S. Kinetic analysis of the non-isothermal degradation of poly(3-hydroxybutyrate) nanocomposites. *Thermochim Acta*. 2008;476:44–50.
- Erceg M, Kovacic T, Klaric I. Thermal degradation and kinetic analysis of poly(3-hydroxybutyrate)/organoclay nanocomposites. *Macromol Symp*. 2008;267:57–62.
- Hablot E, Bordes P, Pollet E, Averous L. Thermal and thermo-mechanical degradation of poly(3-hydroxybutyrate)-based multiphase systems. *Polym Degrad Stab*. 2008;93:413–21.
- Bordes P, Hablot E, Pollet E, Averous L. Effect of clay organomodifiers on degradation of polyhydroxyalkanoates. *Polym Degrad Stab*. 2009;94:789–96.
- Erceg M, Kovacic T, Klaric I. Poly(3-hydroxybutyrate) nanocomposites: isothermal degradation and kinetic analysis. *Thermochim Acta*. 2009;485:26–32.
- Wu TM, Hsu SF, Shih YF, Liao CS. Thermal degradation kinetics of biodegradable poly(3-hydroxybutyrate)/layered double hydroxide nanocomposites. *J Polym Sci, Part B: Polym Phys*. 2008;46:1207–13.

28. Achillas DS, Panayotidou E, Zuburtikudis I. Thermal degradation kinetics and isoconversional analysis of biodegradable poly(3-hydroxybutyrate)/organomodified montmorillonite nanocomposites. *Thermochim Acta*. 2011;514:58–66.
29. Ismail AM, Gamal MAB. Water resistance, mechanical properties and biodegradability of poly(3-hydroxybutyrate)/starch composites. *J Appl Polym Sci*. 2010;115:2813–9.
30. Wang S, Song C, Chen G, Guo T, Liu J, Zhang B, Takeuchi S. Characteristics and biodegradation properties of poly(3-hydroxybutyrate-co-3-3-hydroxyvalerate)/organophilic montmorillonite (PHBV/OMMT) nanocomposite. *Polym Degrad Stab*. 2005; 87:69–76.
31. Naguib HF, Aziz MS, Saad GR. Effect of organo-modified montmorillonite on thermal properties of bacterial poly(3-hydroxybutyrate). *Polym Plast Tech Eng*. 2014;53:90–6.
32. Parkalathan K, Mohanty S, Nayak S. Reinforcing effect and isothermal crystallization kinetics of poly(3-hydroxybutyrate) nanocomposites blended with organically modified montmorillonite. *Polym Compos*. 2014;35:999–1012.